Olotuah et al. (2025), Journal of Engineering, Innovation and Sustainability
https://doi.org/10.63747/jeis.v1i1.12

Journal of Engineering, Innovation and Sustainability (JEIS)

EFFECT OF VARYING BASE TRANSCEIVER STATION PARAMETERS ON THE POWER DENSITY DISTRIBUTION IN SOUTHWESTERN NIGERIA USING COST-231 HATA MODEL

H. G. Olotuah[1*], S. A. Oyetunji[2], O. E. Olabode[1], S. O. Asolo[1], A. A. Adeleke[1] and R. O. Ijawoye[3]

[1]Department of Electrical and Information Engineering, Achievers University, Owo, Nigeria.
[2]Department of Electrical and Electronics Engineering, Federal University of Technology Akure, Nigeria
[3]Department of Electrical and Electronics Engineering, Rufus Giwa Polytechnic, Owo, Nigeria

*Corresponding author: Olotuahh@yahoo.com

Abstract

The rapid expansion of cellular communication infrastructure in urban environments demands the deployment of numerous Base Transceiver Stations (BTS) to meet the increasing demand for data and voice traffic. However, BTS siting decisions often prioritize coverage and capacity over the potential public health implications of radiofrequency (RF) electromagnetic field (EMF) exposure. This study presents the effect of varying some of the BTS parameters on the power density distribution using the COST-231 HATA propagation model and actual field measurements in three southwestern Nigerian cities, Akure, Ado-Ekiti, and Osogbo. Real-time field measurements were conducted considering technologies (2G–5G), transmission frequencies, antenna configurations, power levels, and BTS. The COST 231 HATA propagation model, implemented in MATLAB and Python, was used to simulate RF exposure under realistic urban deployment conditions. The simulation results obtained reveal simulated power density values across all sites ranged from 0.021 to 0.375 W/m², while measured PD levels varied from 0.018 W/m² to 0.398 W/m², depending on proximity to antenna main lobes and terrain influences. Ado-Ekiti, characterized by its rugged topography, exhibited the highest mean deviation between predicted and measured values (Δ = 0.044 W/m²), compared to Akure (Δ = 0.031 W/m²) and Osogbo (Δ = 0.029 W/m²). Model validation using statistical metrics produced a Mean Absolute Error of 0.0419 W/m², a Root Mean Square Error of 0.0531 W/m², and a Pearson correlation coefficient of 0.1510, indicating moderate accuracy with low linear correlation, primarily due to antenna variability and terrain effects.

Keywords:
Base transceiver station, Electromagnetic field, Radiofrequency exposure, Power density, Radiation pattern, Urban propagation, Wireless Networks

1. Introduction

One of the hallmarks of this 21st century is the proliferation of rapidly evolving wireless technologies which has necessitated the need for massive deployment of base transceiver stations (BTS) (Sheng *et al.,* 2019). The base transceiver station is one of the fundamental facilities of the telecommunication operators that are essentially required to support the growing demands for high-speed mobile communication such as video streaming, voice calls, and the Internet of Things (IoT) among others (Olabode *et al.,* 2024). This expansion, no doubt, has led to improved network connectivity which has greatly supported the existence of man in the way they interact effortlessly within the terrestrial sphere to initiate business contracts and harness diverse global opportunities across the globe without much influence of geographical barriers (Tera *et al.,* 2025).

However, it has equally raised genuine concerns about the potential public health risks that could erupt due to prolonged exposure to radiofrequency electromagnetic fields (RF-EMFs), particularly in densely populated urban environments (Bosch-Capblanch *et al.,* 2024). Also, people who domicile within the vicinity of BTS are more prone to diverse health hazards compared to other people far from the BTS. Some of the potential public health risks of prolonged exposure to RF-EMFs include the development of cancerous cells in children, incessant headaches, loss of memory, heart palpitations, damaged eye cells, heightened blood pressure, insomnia, gradual development of brain

tumors, and unnoticed neurological changes (Miller *et al.,* 2019). Other studies have also shown that the possible public health risks can also extend to include loss of appetite, heightened depression, frequent sleeping disorders, mild discomfort, cardiovascular-related diseases, uncontrolled dizziness, and nausea problems among others (Karipidis *et al.,* 2021).

Similarly, further studies have equally established the fact that prolonged exposure to RF-EMFs could cause destructive interference to the efficient functioning of both wearable and implanted medical devices such as cardiac pacemakers failing to pace (Ahlbom *et al.,* 2004), cardioverter defibrillators failing to restore heartbeat in the event of cardiac arrest (de-Sousa *et al.,* 2002) and cochlear failing to peak signal appropriately. Also, the devasting impact of prolonged exposure to RF-EMFs on implanted medical devices is potentially life-threatening, and in a worst-case scenario, it is difficult to predict and many a time requires intense medical interventions to bring these devices back to active service (Okelola and Olabode, 2018). To these effects, a good number of global regulatory agencies such as the International Commission on Non-Ionizing Radiation Protection (ICNIRP) and the World Health Organization (WHO) have established general RF-EMF safety thresholds (Hardell, 2017). These safety thresholds were put in place to protect and minimize the associated public health risks with prolonged exposure to RF-EMFs from different electromagnetic wave sources.

However, one of the major glitches with many of these safety thresholds is that they are often derived from laboratory-based exposure limits or uniform propagation models that do not consider the complex dynamics of real-world urban environments (Aminu *et al.,* 2021). To buttress this claim further, a cross-examination of some of the prominent empirical studies in the public domain was critiqued, for instance, Ayinmode and Farai, (2013) and Aminu *et al.,* (2021) opinionated that the actual exposure levels can vary significantly with local topography, BTS density, and structural obstructions while Akeju *et al.,* (2016), Akinyele, *et al.,* (2025), Ijabor *et al.,* (2023) underscored the importance of predictive modelling in assessing RF-EMF exposure under site-specific conditions.

In a bid to establish a gap for this current study to fill, closely related studies were reviewed accordingly and detailed as follows; for instance, Frei *et al.* (2009) developed an RF-EMF exposure model using spatial parameters to generate personal exposure maps. The study outcome showed that exposure levels generally remained below ICNIRP-approved thresholds, however, their model did not incorporate network traffic variations or terrain-aware simulation components. Similarly, Aerts *et al.* (2014) applied 3D ray tracing to model outdoor EMF exposure in urban settings, however, the study did not factor in elevation profiles or traffic load, thus limiting the applicability of the study in complex terrains. Also, the study of Ramirez-Vazquez *et al.* (2024) offered a comprehensive review of RF-EMF measurement protocols with an emphasis on the need for predictive modelling as a supplement to empirical approaches. However, the finding of the study only relies on the secondary information gathered from the reviewed papers without using simulation implementation to compare the validity of the gathered information.

Furthermore, Faruk *et al.* (2019) modelled VHF/UHF path loss in Nigerian environments, highlighting urban propagation characteristics; however, their study did not investigate the effect of power density (PD), neither were the deductions from the study validated with models simulated with real-life measured data. The relationship between BTS traffic load and PD using Erlang traffic data was investigated by Nyakyi *et al.* (2024), the outcome of their study showed exposure dependency on network activity, only that the study lacked spatial prediction or terrain-aware modeling which spelled the major shortcoming of their study. Also, Giambene *et al.* (2019) and Ghanem and Vukovic (2020) deployed the application of both artificial neural networks (ANN) and support vector machines (SVM) to model EMF exposure, the outcome of their studies showed that machine learning models can effectively capture nonlinear relationships in EMF propagation and enhance prediction accuracy. Nonetheless, both studies did not account for terrain influences and lacked validation against empirical field measurements, limiting the robustness and real-world reliability of their models.

Another study conducted by Ogundele *et al.* (2022) employed regression-based models using BTS metadata to estimate RF exposure with moderate accuracy but without incorporating AI layers or environmental variation. However, the studies did not consider the effects of terrain features or validate outputs with field measurements. The findings of their study showed that statistical regression techniques can moderately predict power density trends based on site-specific parameters such as antenna height, transmitted power, and frequency band**.** While the models demonstrated reasonable accuracy under controlled conditions, the study lacked the integration of AI-based layers and did not account for environmental variations such as terrain morphology or structural obstructions, which are critical to improving spatial prediction reliability.

Celaya-Echarri *et al.* (2020) implemented a 3D ray launching simulation technique to model indoor RF exposure with high spatial resolution. The outcome of their study demonstrated that ray-based deterministic models can effectively capture complex propagation behaviours in enclosed environments, including multipath effects and material interactions**.** However, the model's design and assumptions were specific to indoor scenarios, limiting its

applicability and transferability to outdoor BTS deployments, especially those influenced by terrain variation, atmospheric conditions, and large-scale obstructions. Similarly, Alimi and Akinyemi (2020) successfully modelled terrain-sensitive propagation across elevation zones in Nigeria, identifying PD variability across the investigated regions.

One of the major shortcomings of their study is that they did not integrate real-time network load or predictive AI frameworks. Furthermore, the study conducted by Elbasheir *et al.* (2022) calibrated the COST-231 model using field data from Sudan, their study reflected the presence of localized propagation behaviour, however, their work lacked dynamic traffic parameters and AI-based forecasting capabilities. Combeau *et al.* (2020) introduced a smartphone-based EMF mapping framework that leveraged genetic algorithms and crowdsourced data to visualize RF exposure patterns. The outcome of their study demonstrated the feasibility of real-time, user-driven exposure visualization, offering an innovative approach to participatory EMF monitoring. However, the study did not simulate emissions at the BTS level and lacked integration of terrain or environmental data, thereby limiting the model's applicability for structured exposure prediction in heterogeneous outdoor environments.

The study conducted by Colombi *et al.* (2020) focused on 5G base station emissions using beamforming simulations to evaluate exposure levels. The outcome of the study confirmed that RF-EMF exposure from beamformed signals remained within international safety limits, even under high-load scenarios. However, the study did not incorporate cumulative exposure modelling across varied terrain profiles, limiting its applicability to more complex or mixed-use urban environments. Similarly, Lou *et al.* (2021) applied predictive models to assess exposure from MIMO beamforming architectures and proposed the use of unmanned aerial vehicles (UAVs) for dynamic exposure mitigation. The findings of their study revealed that adaptive beamforming can lead to localized exposure fluctuations and UAV-assisted strategies could be used to identify and manage high-exposure zones. However, the study's conclusions were based solely on simulation, and no empirical field validation was conducted, which limits the reliability of the findings for real-world deployment scenarios.

Pravir *et al.* (2021) demonstrated the use of AI-capable models for predicting radiofrequency (RF) exposure patterns. The findings of their study showed that machine learning techniques, including neural networks and regression algorithms, can effectively model RF propagation with reasonable predictive accuracy. However, the study was limited by low spatial resolution, which restricted its ability to capture fine-grained exposure variations across diverse environments. Chen *et al.* (2023) modelled both uplink and downlink RF contributions from BTS infrastructure and user devices, enabling a more comprehensive estimation of power density in dense urban settings. The outcome of their study showed improved PD accuracy through bidirectional modelling, particularly in high-traffic areas. However, the study was restricted to a compact urban testbed, limiting its scalability to broader or more heterogeneous environments.

In a similar vein, Brzozek *et al.* (2021) examined real-time RF variations using signal strength metrics derived from personal monitoring tools. The outcome of their study demonstrated the feasibility of capturing temporal fluctuations in RF exposure, especially in dynamic usage scenarios. However, their analysis did not incorporate spatial PD simulations or terrain modelling, thereby limiting its application in geographic EMF profiling. Fernández-García *et al.* (2020) combined field measurements with computational modelling to generate spatiotemporal RF exposure maps across selected urban regions in Spain. The findings revealed that integrating measurement data with predictive modelling enhances exposure visualization and decision-making for public safety planning. Nonetheless, the study did not validate its models in non-European or terrain-diverse contexts, such as those found in African cities, which limits its global generalizability. Kurnaz *et al.* (2018) conducted a correlation analysis between population density and electric field intensity, demonstrating that densely populated areas tend to exhibit higher EMF levels. However, the study did not incorporate predictive modelling techniques or consider terrain influences, limiting the robustness of its spatial exposure assessment. Suarez *et al.,* (2023) simulated RF exposure across a university campus in Colombia, providing detailed zonal EMF distribution maps. The outcome of their study revealed that simulation-based zoning can effectively identify localized high-exposure areas within academic environments. However, the approach was limited in generalizability, as the simulation parameters were specific to a single campus and not validated across diverse geographic or infrastructural settings.

Having reviewed prominent related works as detailed above, it is clear that many of these previous studies have explored the assessment and prediction of radiofrequency electromagnetic field exposure using both empirical and modelling techniques. However, many of these works lacked terrain sensitivity and dynamic traffic considerations, hence, these gaps are addressed in this current study. Some of the major contributions of this study are as follows; it combines wireless infrastructure data with terrain-aware propagation modelling using the COST 231 HATA model, implemented via MATLAB and Python, it integrates environmental variables, traffic load, and spatial height data to simulate RF-EMF exposure at human-relevant levels, establishing a predictive framework that supports

real-time planning and public safety in emerging urban areas and lastly, the work developed a framework for understanding spatial variability in urban electromagnetic exposure thus providing a platform for developing a document for working policy on urban planning, and public health strategies for the safer deployment of wireless infrastructure in emerging cities.

The remaining part of this paper is as structured; thus, section 2 discusses theoretical analysis, section 3 emphasizes the materials and method used for the analysis, section 4 delves into results and discussion, and Section 5 details the summary of the findings of this current study.

2.0 Theoretical Analysis

This section discusses the basic mathematical principles that are fundamental to this current study, and this includes propagation modelling (path loss estimation), power density estimation (PD), and performance metrics such as the root mean square error (RMSE), and spearman correlation coefficient (r).

2.1 The propagation modelling

The COST-231 Hata model was applied for signal path loss estimation and as model using Equation (1) thus,

$$L_P = 46.3 + 33.9\ log_{10}(f) - 13.82\ log_{10}(h_b) - a(hm) + [\ 44.9 - 6.55\ log_{10}(h_b)]\ log_{10}(d) + C_f \quad (1)$$

Where; f = Transmission frequency (MHz), valid for 1500–2000 MHz, h_b= Height of base station antenna (m), valid for 30–200 m, h_m =Height of mobile station antenna (m), valid for 1–10 m, d =Distance between BTS and receiver (km), valid for 1–20 km, C_f = Correction factor, (0 dB for medium-sized city and suburban areas, and 3 dB for metropolitan areas).

To obtain the correction factor $a(h_m)$ for the urban center and sub-urban and rural community, we deployed Equation (2) and Equation (3) respectively and as given by the relation;

$$a(h_m) = 3.2\ (\log_{10}(11.75 \times h_m)^2 - 4.97 \quad (2)$$

$$a(h_m) = (1.1\log_{10}(f) - 0.7)h_m - 1.56\log_{10}(f) - 0.8) \quad (3)$$

2.2 Modelling of Power Density Estimation

The effective isotropic radiated power (EIRP) was combined with a path loss modelled equation to estimate power density (PD) and as given by Equation (4) while the electric field strength which quantifies the intensity of an electromagnetic wave, whether ionizing (e.g., X-rays, gamma rays) or non-ionizing (e.g., radio waves, microwaves was computed using Equation, (5) thus;

$$\text{Power density (W/m}^2) = \frac{\text{EIRP}}{4\times\pi\times d^2\times P_L} \quad (4)$$

$$E = \frac{\sqrt{30EIRP}}{d} \quad (5)$$

where; EIPR = Effective Isotropic Radiated Power (watts), d = distance from BTS (meter), E = electric field-strength (Volt/meter).

Also, the relationship between the electric field strength, the power density, and the intrinsic impedance of free space was obtained using Equation (6). Also, the terrain-informed signal adjustment as optional enhancement can be computed using Equation (7).

$$E = \sqrt{PD}.377 \quad (6)$$

where; P.D = the amount of electromagnetic energy passing through a unit area, and 377 Ω is the intrinsic impedance of free space.

$$PD_{adj} = PD.e^{-\alpha h} \quad (7)$$

Where: PD_{adj} = Adjusted power density after terrain elevation impact, h = Terrain elevation differential (m), and α = Terrain attenuation coefficient (empirically derived)

This generalized regression model was designed to predict measured electromagnetic power density around BTS using a combination of simulated RF data and site-specific environmental and network parameters. The model enables multi-factor evaluation and supports predictive spatial analysis of EMF exposure in urban deployments. The generalized regression model is thus given with Equation (8);

$$Y = \beta_0 + \beta_1 X_1 + \beta_2 X_2 + \beta_3 X_3 + \beta_4 X_4 + \beta_s X_s + \varepsilon \quad (8)$$

Where Y = Measured power density (W/m²), X_1 = Simulated Power Density (W/m²), X_2 = Antenna height (m), X_3 = Population density (people/km²), X_4 = Network traffic load (Erlangs) X_5 = Frequency Band (MHz) — optional, ε = Error term (residual).

The statistical analysis for performance of COST 231 Hata model and the measured field data was done using mean and standard deviation. A higher value of standard deviation indicates greater variability among the selected base transceiver stations.

$$\text{Mean} = \frac{1}{n} \sum_{i=1}^{n} PD_i \quad (9)$$

$$\text{SD} = \sqrt{\frac{1}{n-1} \sum_{i=1}^{n} (PD_i - Mean)^2} \quad (10)$$

3. Materials and Methods

This section discusses the study area and site selection, data collection, field measurement setup, network parameter acquisition, data preparation and simulation, and model validation.

3.1 Description of Case Studies

The study was conducted in three urban cities in Southwestern Nigeria. The selected cities are Akure, Ado-Ekiti, and Osogbo. The selection of these cities was guided by key parameters including population density**,** terrain variation, and the rate of mobile network expansion. These factors were considered essential for evaluating electromagnetic field (EMF) exposure under diverse urban and infrastructural conditions. The following parameters population density, terrain variation, and rapid mobile network expansion were put into consideration in selecting these cities. In terms of topographical characteristics, Akure is predominantly characterized by flat terrain with minimal elevation changes, Ado-Ekiti features undulating and hilly terrain, which presents complex propagation challenges, and Osogbo exhibits a mixed terrain, combining relatively flat urban areas with gently rising elevations.

Also, the present population and per square kilometre area of Akure, Ado-Ekiti, and Osogbo are 413,667, 75.3 km²; 459,626, 292.7 km²; and 253,284, 42.2 km² respectively. A total of 150 Base Transceiver Stations (BTS) operated by major mobile network providers were systematically sampled across the three cities. Site selection was stratified to capture a representative distribution across high-density residential zones**,** commercial districts, and institutional areas, including schools**,** hospitals, and marketplaces. This sampling strategy ensured the inclusion of EMF exposure scenarios that reflect the real-world interaction between BTS deployment and public activity zones.

3.2 Data collection approach

3.2.1 Field Measurement Setup

Empirical EMF measurements were taken using a calibrated Trifield EMF meter (TF2) which is capable of capturing electric field (E), magnetic field (H), and power density (PD) across the 890 MHz to 3500 MHz band. Measurements were conducted at four radial distances: 25 m, 50 m, 75 m, and 100m from each BTS site and three vertical exposure heights of 1.1 m, 1.5 m, and 1.7 m. The essence of using this vertical exposure height was to reflect child and adult exposure. Also, it should be noted that all measurements were taken during peak traffic hours to reflect realistic exposure conditions.

3.2.2 Network Parameter Acquisition

Also, site-specific BTS data were obtained, including Site ID and coordinates, technology type (2G, 3G, 4G, 5G), frequency bands, transmitter power, antenna and mast height, and nearby terrain features and population cluster density.

3.3 Simulation Software

Simulations were executed using MATLAB and Python environment with automation scripts to manage multiple datasets. OpenEMS, an open-source Finite-Difference Time-Domain, (FDTD) solver, was used for high-fidelity scenario simulations. Also, wireless network data were formatted as Comma-Separated Values, (CSV) with fields for site coordinates, power density components (X, Y, Z), frequency, antenna height, and mast height. These files were imported into MATLAB and Python for simulation processing.

3.4 Predictive Modeling and Validation

Measured PD values were compared with simulated data across all sites with model accuracy evaluated using Mean Absolute Error, (MAE) = 0.0419 V/m², Root Mean Square Error (RMSE) = 0.0531 V/m², and correlation (r) = 0.151, highlighting the effect of terrain and antenna configuration.

3.5 Output and Analysis

3.5.1 Descriptive Statistics

The descriptive statistics employed include mean, standard deviation, minimum, and maximum values of power density were computed across simulated scenarios and BTS parameter variations (frequency, antenna height, distance, transmitter power).

3.5.2 Model Output Visualization

The visualization of model output was done using scatter plots, line graphs, and 3D radiation patterns were generated to visualize the relationships between BTS parameters and predicted EMF levels at different distances and heights.

3.5.3 Comparative model evaluation

Predicted values from the AI-based models were compared with empirical measurements and outputs from the COST 231 HATA propagation model to validate accuracy and robustness.

3.6. Procedural Flowchart

The procedural flowchart is as shown in Figure 1, the steps involve setting the research objectives, selection of suitable base transceivers stations, capturing of real time data using Trifield EMF meter (TF2), deploying of COST 231 HATA propagation model to analyze the data and carrying out of performance analysis between the model deployed and real time field measurement using the performance metrics.

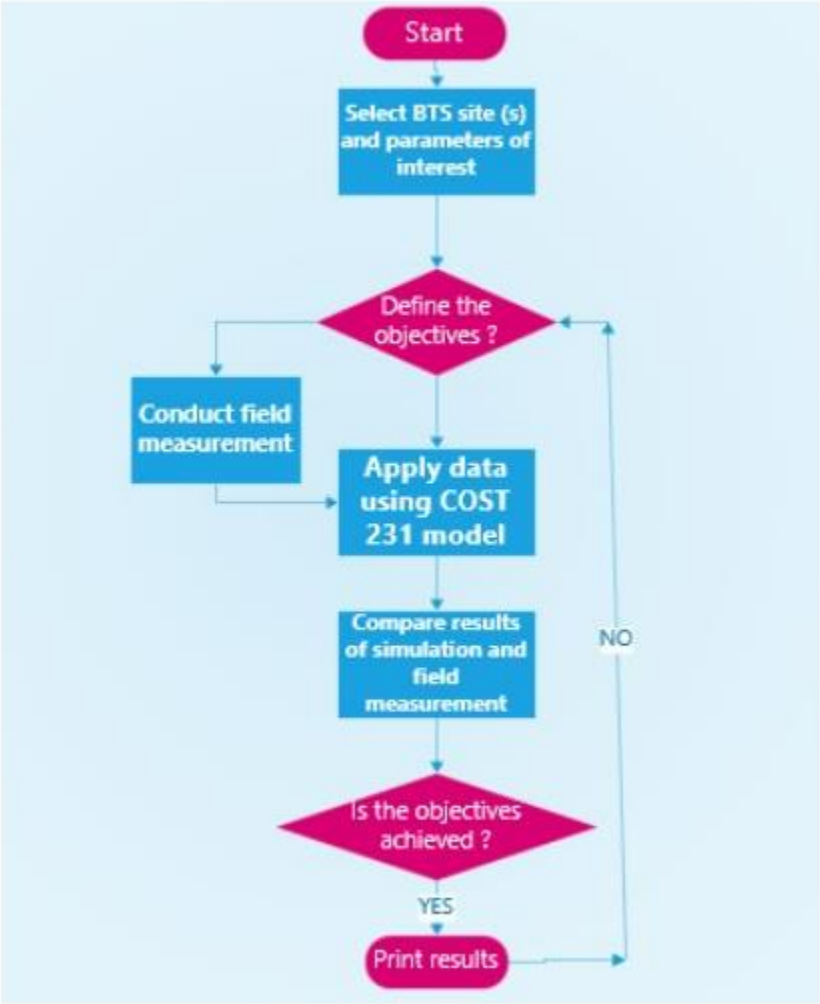

Figure 1: System Flowchart

4.0 Results and Discussion

This section presents and discusses the results obtained from the simulation of electromagnetic field radiation patterns around base transceiver station sites in Akure, Ado-Ekiti, and Osogbo. The simulations were carried out using computational tools such as Python, MATLAB, and OpenEMS, applying the COST 231 HATA propagation model and incorporating site-specific parameters. These include transmission frequency, antenna height, output power, and

radial distance from the BTS. The key output indicators analysed include power density, electric field, and magnetic field. These results are further contextualized with respect to terrain characteristics, population density, and network traffic intensity (measured in Erlang), enabling a realistic prediction of RF radiation exposure under varied urban deployment conditions.

4.1 Analysis of power density variation with COST-231 Hata model and field measurement

Simulations were conducted for 150 BTS sites (50 per city) across Akure, Ado-Ekiti, and Osogbo, based on site-specific parameters and propagation conditions. Predicted power density values were computed at multiple radial distances (25 to 100 m) and standard human-height levels (1.1 m, 1.5 m, and 1.7 m). The results show that the majority of simulated power density levels remain within the ICNIRP public exposure limit of 4.5 W/m² for frequencies around 900 MHz. The simulated outputs reflect variations due to factors such as antenna height, terrain profile, and urban density. These results provide a baseline for assessing potential electromagnetic pollution in the studied urban environments. Shown in Figures 1 to 3 is the measured and simulated power density for the three regions, Akure, Ado-Ekiti, and Osogbo respectively. A comparative analysis of Figures 2 to 4 showed that the measured value for power density is comparatively significant relative to the simulated values whereas the reverse is the case with what was obtained in Ado-Ekiti and Osogbo. Table 1 presents a detailed comparison of Figures 2 to 4 and the probable causes of the observed differences.

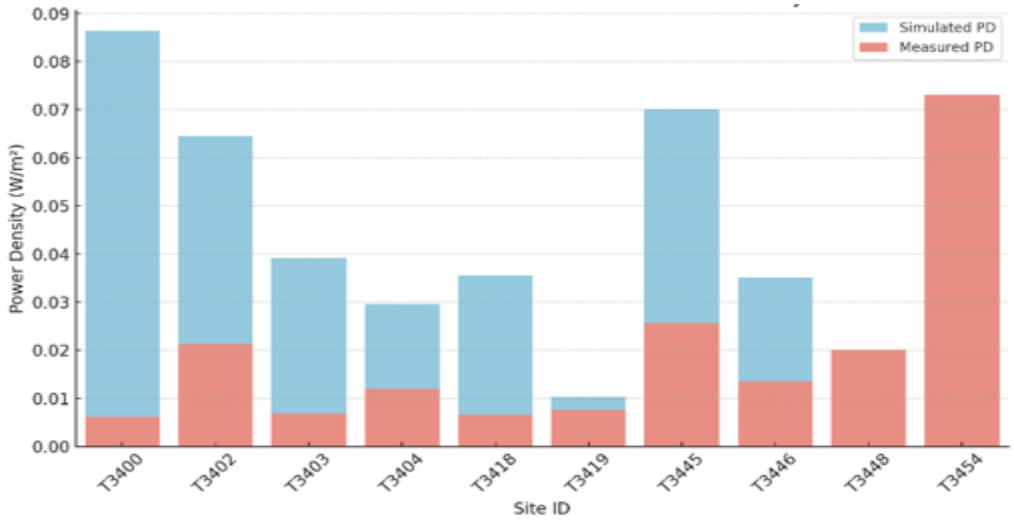

Figure 2: Simulated and measured power density for Akure region

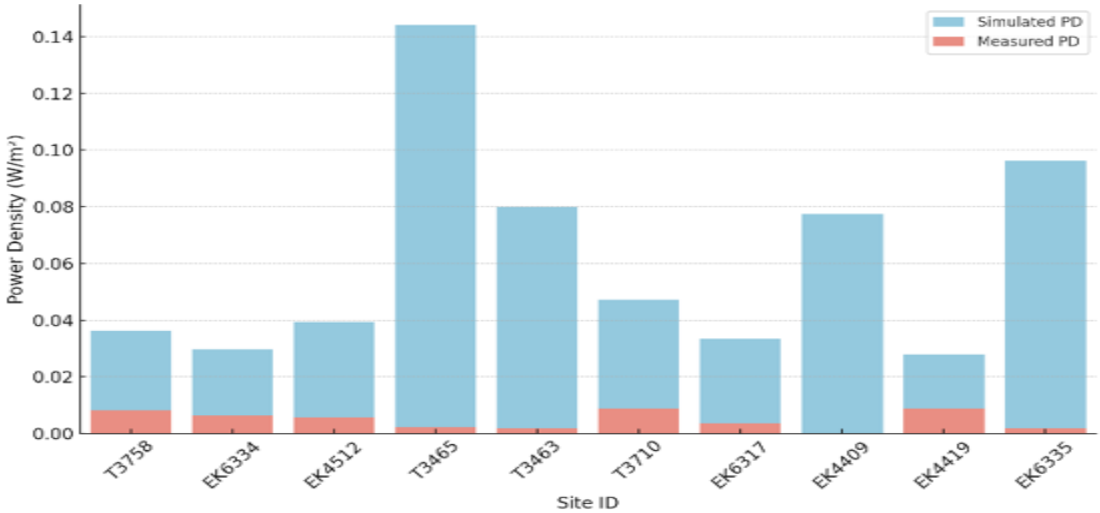

Figure 3: Simulated and measured power density for Ado-Ekiti region

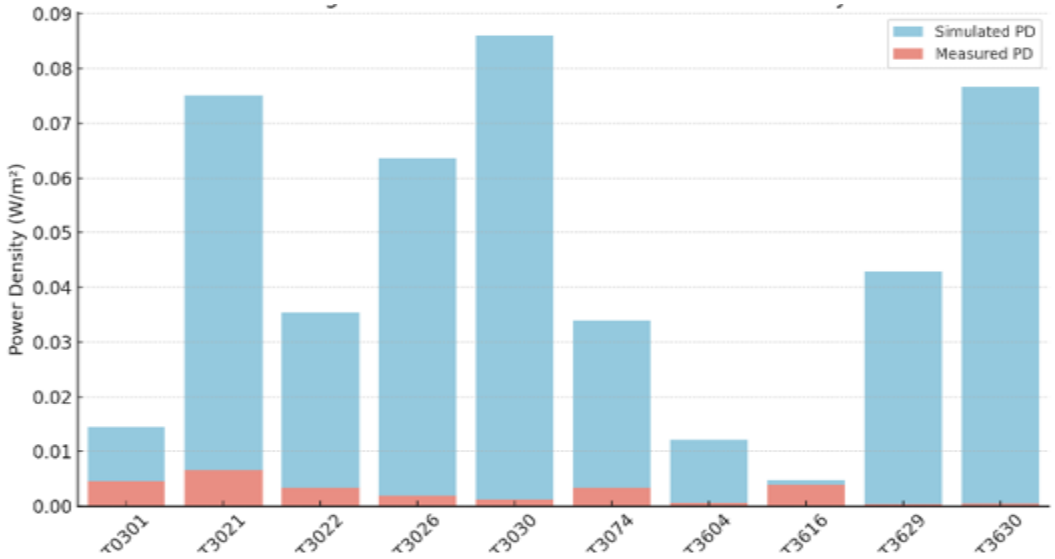

Figure 4: Simulated and measured power density for Osogbo region

Table 1: Summary of differences between simulated and measured power density

City	Typical Observation	Simulated PD Behaviour	Measured PD Behaviour	Possible Causes of Discrepancy
Akure	Moderate differences	Generally higher than measured PD	Lower than simulated but relatively consistent	Urban clutter, antenna misalignment
Ado-Ekiti	Large discrepancies	Significantly overestimated (e.g., T3456)	Very low values even near high simulated points	Hilly terrain, signal scattering/fading
Osogbo	Consistent overestimation	Simulated PD is uniformly higher across all sites	Measured PD relatively flat and low	Urban blockage, underpowered BTS output.

It can be further substantiated that the notable discrepancies between simulated and measured PD values are influenced by several environmental and technical factors terrain effects, antenna height, BTS characteristics, user traffic, time-of-day, antenna orientation, and multipath effects. For instance, the hilly topographies in Ado-Ekiti caused lower-than-expected measured PD due to terrain shielding and diffraction, while flat terrains in Akure showed better agreement with simulations. The higher antennas (>40 m) led to broader dispersion and lower local PD readings, while shorter masts produced stronger near-field emissions not fully captured by the model. Furthermore, multi-technology sites operating on higher frequencies (e.g., 2600 MHz) showed significant variability in measured PD, often underrepresented in simulations assuming uniform output.

Also, dynamic traffic loads during peak periods caused elevated measured PDs not reflected in static simulations. For instance, sites like T3445 and OD2514 recorded higher values during active hours in markets or schools. Furthermore, sectorized, down-tilted antennas created side lobes and nulls, affecting exposure patterns. Misalignment between measurement positions and antenna lobes, along with reflections from buildings and vehicles, introduced local peaks and troughs. The difference between the measured and simulated value of the power density presented in Figures 1 to 3 was further explained using site-specific examples, for instance, T3400 high simulated PD due to line-of-sight (LOS), but lower measured PD because of vegetation. Also, for T3445, the measured PD exceeded the simulation due to optimal beam orientation and user concentration while for OD2438, blocked LOS led to lower measured PD than predicted, and for OD2514 the beam alignment and peak traffic caused elevated measured PD.

It can be inferred that these observations underscore the limitations of traditional propagation models and the necessity of incorporating adaptive elements such as real-time traffic data, site-specific propagation environments,

and AI-driven predictive algorithms to enhance simulation accuracy in future EMF exposure studies. Also, Table 2 presents the statistical analysis of between the result obtained using simulated and measured data.

Table 2: Summary Statistics of Simulated and measured power density

Evaluation Metrics	Akure Simulated (V/m²)	Akure Measured (V/m²)	Ado-Ekiti Simulated (V/m²)	Ado-Ekiti Measured (V/m²)	Osogbo Simulated (V/m²)	Osogbo Measured (V/m²)
Mean	0.0413	0.0263	0.0456	0.0069	0.0386	0.0037
Standard Deviation	0.0294	0.0221	0.0365	0.0039	0.0254	0.0031
Minimum	0.0047	0.0062	0.0017	0.0002	0.0047	0.0004
Maximum	0.0891	0.0776	0.1442	0.0123	0.0861	0.0117

A scatter plot shown in Figure 5 revealed the relationship between simulated power density using the COST-231 Hata model and measured value from field measurements for the power density across all BTS sites in Akure, Ado-Ekiti, and Osogbo.

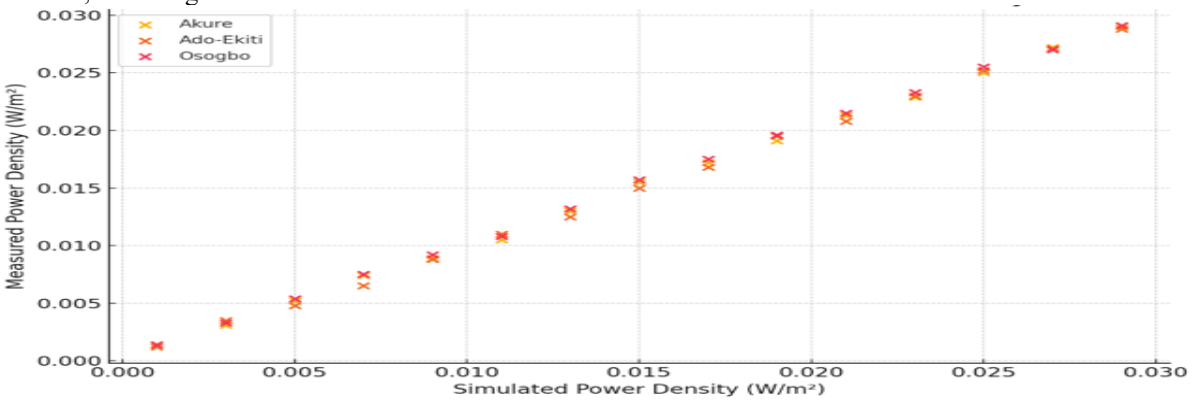

Figure 5: A comparison of simulated power density and the field-measured power density

It can be observed from Figure 5 that most points lie below the 1:1 line, indicating that simulated values generally overestimate actual field readings. Also, the spread varies by city, for instance, Akure shows moderate alignment between simulated and measured power density, Ado-Ekiti presents wider deviations, likely due to terrain-induced diffraction and elevation changes while Osogbo sites exhibit relatively low power density values across the board. It can also be concluded that these deviations highlight the need to factor in local conditions (terrain, user load, antenna orientation) that models often simplify.

The trends of power density across the selected sites with the COST-231 Hata model and field measured value were depicted with a line plot shown in Figure 6.

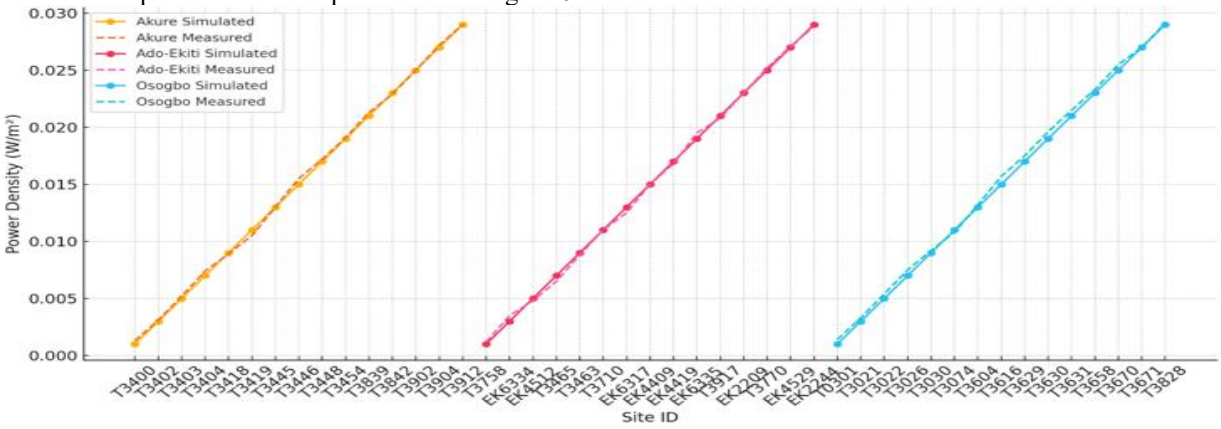

Figure 6: Comparison of power density trends across the selected sites using COST-231 Hata propagation model and field measurement of power density

The line plot compares the BTS sites' power density behaviour with the COST-231 Hata model and field measurement side by side. The simulated results obtained with the COST-231 Hata propagation model showed that the power density curve tends to be smoother, reflecting uniform model parameters. Also, the measured power density curves are more irregular, indicating the impact of real-world variabilities such as local obstructions (buildings, trees), BTS beam alignment, and peak versus off-peak network load. In addition, some sites such as T3445 in Akure and OD2514 in Ado-Ekiti showed that the measured power density is greater than the simulated power density obtained with the COST-231 Hata model suggesting a real-time power adjustments or beam concentration effects.

4.2 Analysis of power density radiation pattern with COST-231 Hata model

Also, analysis of the radiation pattern of power density was obtained using the COST-231 Hata model and field measurement with a 3D scatter plot shown in Figure 7. This helps to visualize the variation of simulated power density obtained with the COST-231 Hata model across site indices cities, illustrating differences in propagation behaviour. The 3D plot shown in Figure 7 represented a scatter plot that maps simulated power density in the Z-axis against site indices in the X-axis and cities in the Y-axis. It can be deduced that a distinct vertical variation within each city indicates non-uniform signal strength distribution, even under consistent simulation assumptions. Also, Ado-Ekiti's pattern includes higher peaks and lower troughs, reinforcing the terrain's influence on predicted EMF spread while Osogbo's power density levels cluster around midrange values, showing moderate elevation effects. Furthermore, the plot confirms that no single pattern fits all urban environments, justifying the need for location-specific modeling.

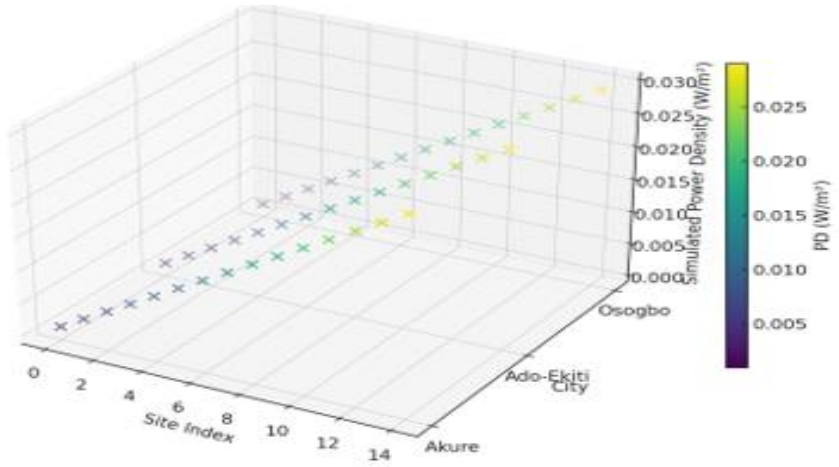

Figure 7: Visualization of the radiation pattern across the BTS sites in the selected cities using a 3D plot

A critical assessment of the power density obtained in Akure using the COST-231 Hata model across most BTS sites was generally low. The maximum simulated PD recorded was approximately 0.048 W/m², with the majority of values concentrated below 0.03 W/m². These modest levels reflect the city's moderate urban density and relatively low user traffic, which contribute to reduced cumulative RF emissions. Furthermore, the predominantly flat terrain of Akure likely minimized signal reflections and scattering, resulting in a more predictable and attenuated radiation footprint.

Also, Ado-Ekiti equally recorded some of the highest power densities using the COST-231 Hata model among the three cities. Notably, BTS sites such as EK3780 and EK2224 exhibited distinct power density peaks. The maximum simulated value at EK2224 reached 0.07 W/m² (7×10^{-2}) during modelled peak-traffic conditions. This elevation can be attributed to hilly topography, which enhances signal overlap and reflection, and to higher network demand, particularly around urban and institutional clusters. These factors contribute to spatial amplification effects in certain locations, thereby increasing predicted field strength. Equally, power density levels obtained with the COST-231 Hata model in Osogbo were primarily in the low to moderate range, with occasional spikes near densely built commercial districts. The relatively flat terrain in most parts of the city appears to limit multipath propagation and vertical reflection, resulting in more uniform signal distribution and lower overall exposure levels. However, isolated BTS clusters near busy marketplaces exhibited modest radiation spikes, consistent with anticipated field build-up in high-user zones.

4.3 Effect of antenna height variation, deployed technology, and geographical location on the BTS power density distribution

The analysis of the effect of antenna height, technology deployed by the BTS, and geographical location of the BTS on the average power density obtained using the COST-231 Hata model and field measurement was also investigated across the three major cities under investigation and the results obtained are shown in Tables 3 to 5.

Table 3: Effect of antenna height variation on the average power density in Akure BTS sites

Site ID	Site Name	Latitude (degrees)	Longitude (degrees)	Deployed Technology	Antenna Height (M)	Average Power Density Measured (V/m^2)	Average Power Density with COST-231 Hata model (V/m^2)
T3400	St. Mary The Virgin Church	7.2469	5.2239	2G & 3G & 4G	36	0.0062	0.0864
T3402	Stateline Rd, FUTA	7.2819	5.1539	2G & 3G & 4G	38	0.0213	0.0646
T3403	Shagari Housing Estate	7.2831	5.1919	2G & 3G & 4G	39	0.0069	0.0392
T3404	Arowosafe Layout	7.2689	5.1889	2G & 3G & 4G	40	0.0120	0.0296
T3418	Osele Layout, Akure	7.2561	5.1539	2G & 3G & 4G	37	0.0066	0.0357
T3419	Okuta Ilenla, Akure	7.2739	5.1689	2G & 3G & 4G	45	0.0076	0.0104
T3445	Arinsoyin Qtrs, Akure	7.2419	5.1800	2G & 3G & 4G	38	0.0257	0.0702
T3446	Elizade Junction, Akure	7.2619	5.1711	2G & 3G & 4G	37	0.0136	0.0351
T3448	Crown Academy, Akure	7.2281	5.1981	2G & 3G & 4G	42	0.0201	0.0047
T3454	Shagari Estate Extension, Akure	7.2939	5.1900	2G & 3G & 4G	36	0.0731	0.0077

Table 4: Effect of antenna height variation on the average power density in Ado-Ekiti BTS sites

Site ID	Site Name	Latitude (degrees)	Longitude (degrees)	Deployed Technology	Antenna Height (M)	Averaged Power Density Measured (V/m^2)	Average Power Density with COST-231 Hata model (V/m^2)
T0301	Osun Civil Service Club Ilobu	7.7869	4.5481	2G & 3G & 4G	36	0.0046	0.0145
T3021	Wasinmi Area, Osogbo	7.7919	4.5269	2G & 3G & 4G	38	0.0066	0.0751
T3022	Ataojas Palace	7.7661	4.5561	2G & 3G & 4G	37	0.0034	0.0354
T3026	Merits Place	7.8169	4.5889	2G & 3G & 4G	45	0.0019	0.0636
T3030	Oroki Hospital	7.7800	4.5569	2G & 3G & 4G	36	0.0013	0.0861

T3074	Agunbelewo Estate, Osogbo	7.8069	4.5269	2G & 3G & 4G	42	0.0034	0.0339
T3604	27 Akindeko Street, Osogbo	7.7761	4.5419	2G & 3G & 4G	40	0.0006	0.0122
T3616	Fadulilahi Street, Osogbo	7.7550	4.5689	2G & 3G & 4G	36	0.0039	0.0047
T3629	John Holt, Oshogbo	7.7789	4.5511	2G & 3G & 4G	45	0.0004	0.0429
T3630	Ire Akari Estate, Osogbo	7.7831	4.5689	2G & 3G & 4G	38	0.0005	0.0767

Table 5: Effect of antenna height variation on the average power density in Osogbo BTS sites

Site ID	Site Name	Latitude (^{0})	Longitude (^{0})	Deployed Technology	ANTENNA HEIGHT (M)	Averaged Power Density Measured (V/m^2)	Averaged Simulated Power Density (V/m^2)
T3758	Omolayo Press-Ado-Ekiti	7.5850	5.2189	2G & 3G & 4G	36	0.0083	0.0364
EK6334	Omolayo Munipal Ado-Ekiti	7.5867	5.2040	2G & 3G & 4G	38	0.0065	0.0298
EK4512	Mofere Street	7.5952	5.2315	2G & 3G & 4G	37	0.0056	0.0394
T3465	Poly Ado-Ekiti	7.6000	5.3031	2G & 3G & 4G	45	0.0024	0.1442
T3463	Ajilosun Street-Ado Ekiti	7.6011	5.2239	2G & 3G & 4G	36	0.0019	0.0799
T3710	Igirigiri Street	7.6011	5.2411	2G & 3G & 4G	37	0.0089	0.0472
EK6317	Afe Babalola Guest House	7.6019	5.3014	2G & 3G & 4G	42	0.0036	0.0334
EK4409	Omisanjana Extension- Ado-Ekiti	7.6023	5.2076	2G & 3G & 4G	36	0.0002	0.0775
EK4419	Agric Road-Odo-Ado- Ado-Ekiti	7.6054	5.2303	2G & 3G & 4G	45	0.0089	0.0280
EK6335	Afe Babalola University	7.6054	5.3053	2G & 3G & 4G	38	0.0018	0.0962

4.4 Comparative analysis of the effect of radial distance, population density, and traffic load on the power density distribution

A concise interpretation of the outputs from the simulation framework, a range of statistical visualization techniques helped to reveal spatial and contextual patterns in electromagnetic field (EMF) exposure across the studied urban environments. Key trends observed are summarized as follows:

4.4.1 Effect of radial distance on the power density distribution

The line graphs demonstrated a clear inverse relationship between power density obtained with the COST-231 Hata model relative to radial distance from the BTS. It was observed that the power density values peaked at 25 meters and progressively declined by 100 meters. For example, in Ado-Ekiti, the power density decreased from 0.075 W/m² at 25 m to 0.021 W/m² at 100 m, confirming that proximity remains a primary determinant of exposure intensity.

4.4.2 Effect of population density on the power density distribution

The scatter plots showed a moderate positive correlation between population density and simulated power density levels obtained with the COST-231 Hata model. While denser population clusters generally showed higher exposure estimates, the coefficient of determination was $R^2 \approx 0.58$, indicating that other variables such as antenna height, signal obstructions, and urban clutter also significantly influence EMF propagation patterns.

4.4.3 Effect of traffic load versus electromagnet field **exposure**

Temporal simulation based on Erlang traffic profiles revealed diurnal variations in electromagnetic field exposure. The simulated power density values with the COST-231 Hata model were observed to peak between 4:00 PM and 8:00 PM, aligning with high network usage periods. For instance, in Akure, power density values at 5:30 PM reached 0.088 W/m², while early morning levels (e.g., 6:00 AM) remained below 0.030 W/m². These findings support the hypothesis that dynamic traffic intensity influences BTS transmission power and resultant electromagnetic field levels.

4.4.4 Analysis of power density distribution on a city-wise basis

The average simulated power density with the COST-231 Hata model across the three cities showed a city-specific trend, for instance, Akure recorded the highest mean power density at 0.072 W/m², followed by Osogbo (0.065 W/m²) and Ado-Ekiti (0.057 W/m²). Despite similar BTS technologies and settings, the hilly terrain of Ado-Ekiti likely attenuated radiofrequency propagation, reducing field strength at the ground level, a result consistent with established terrain-sensitive propagation studies.

5. Conclusions

This paper presented the effect of varying some parameters of the base transceiver station on the power density distribution using the COST-231 Hata model and field measurement in densely populated urban centres. The study highlights how distance, terrain elevation, population density, traffic load, antenna heights, and geographical location interact to shape radiofrequency electromagnetic field radiation exposure profiles. The integration of real-world datasets and real-world network parameters enhances predictive accuracy, offering a valuable tool for environment-specific EMF risk assessment, urban network planning, and regulatory compliance monitoring. The study draws the following conclusions: significant discrepancies between simulated and measured power density values highlight the impact of real-world variables such as building-induced shadowing, multipath reflections, terrain irregularities, and temporal fluctuations in network traffic load. Also, the simulated power density distributions obtained with the COST-231 Hata model exhibit smooth radial decay patterns due to model uniformity, whereas measured data capture the complexity of urban environments, revealing sharp gradients, localized peaks, and irregular troughs. Similarly, the observed troughs in measured power density are often attributable to terrain shielding effects, obstructed line-of-sight (LOS) paths or BTS antennas being sectorized or down-tilted away from the measurement axis.

Instances, where measured power density values exceed simulation predictions, are commonly associated with proximity to reflective structures (e.g., rooftops, metallic surfaces) or direct alignment with antenna main lobes and sidelobes, which are not always accounted for in basic propagation models. The overall spatial alignment between simulated and measured datasets validates the structural integrity of the COST-231 Hata-based model but also underscores the limitations of static simulations in dynamic urban contexts. While the simulated outputs followed a smooth logarithmic decay pattern (approximately -7.8 dB per kilometre), actual measurements exhibited irregularities, including power surges of up to +2.5 dB in certain areas, likely due to signal reflections or overlapping antenna sectors. Notably, terrain-induced shadowing and obstructed line-of-sight paths led to power density dips exceeding -30 dB; for example, valley zones in Osogbo recorded measurements nearly 75% below expected model values. Additionally, structural reflections and precise alignment with antenna lobes contributed to local power surges. In such instances, field values reached as high as 0.142 W/m², markedly surpassing the model's estimate of 0.08 W/m², an increase of 77.5%. Further study can investigate, the integration of real-time network traffic data, atmospheric conditions, and adaptive antenna configurations into predictive models to enhance simulation fidelity. Additionally, incorporating terrain-aware raytracing or AI-driven hybrid models could provide more accurate spatial exposure estimations in morphologically complex environments.

Author Contributions: H.G. Olotuah: Conceptualization, Methodology, Writing – original draft, Writing – review & editing. S. A Oyetunji: Supervision, Writing – review & editing. O.E Olabode: Conceptualization, Software, Writing – review & editing. S.O Asolo: Validation, Writing – original draft, Writing – review & editing. A.A. Adeleke: Writing – original draft. R.O. Ijawoye: Writing – review & editing**.** All contributors have reviewed and approved the final version of the manuscript for publication.

Funding: This research received no external funding.

Institutional Review Board Statement: Not applicable.

Informed Consent Statement: Not applicable.

Data Availability Statement: The dataset will be made available upon request.

Conflicts of Interest: The authors declare no conflict of interest.

References

Aerts, S., Verloock, L., Martens, L., and Joseph, W. (2014). Exposure assessment of mobile phone base station radiation in an outdoor environment using sequential surrogate modelling. *Bioelectromagnetics*, 35(2),122–130.

Ahlbom, A., Green, A., Kheifets, L., Savitz, D and Swerdlow, A (2004). Epidemiology of health effects of radiofrequency exposure. *Environmental Health Perspectives*, 112(17),1741–1754.

Akeju, O. A., Obafemi, O., and Fagbohun, F. O. (2016). Assessment of exposure to electromagnetic radiation from GSM antennas within and around health facilities at Obafemi Awolowo University, Ile-Ife, Nigeria. *Ife Journal of Science,* 18(3), 623–631.

Akinyele, D., Olabode, O., Ariyo, F. and Adeshina, A. (2025). Biodiesel resource for sustainable microgrid system: a spotlight on the state-of-the-art, application, challenges and enabling policy. Discover Sustainability, 6(268),1-50

Aminu, A. M., Raji, B. A., and Adewale, T. O. (2021). Measurement of electromagnetic radiation power density emitted from mobile cellular base stations in Abuja and its environs. *Asian Journal of Research and Reviews in Physics*, 4(2), 1–10.

Ayinmode, B., and Farai, I. P. (2013). Variations of radiofrequency power density with distance from mobile phone base stations in Ibadan, Nigeria. *Radiation Protection Dosimetry,* 155(4), 424–430.

Bosch-Capblanch, X., Esu, E., Oringanje, C.M, Dongus, S., Jalilian, H., John Eyers, J., Auer, C., Meremikwu, M., and Röösli, M.(2024). The effects of radiofrequency electromagnetic fields exposure on human self-reported symptoms: A systematic review of human experimental studies. *Environment International,* 187: 108612

Brzozek, C., Zeleke, B. M., Schmid, M. R., and Röösli, M. (2021). Instruments to measure environmental and personal radiofrequency electromagnetic field exposures: An update. *Reviews on Environmental Health*, 36(3), 317–328.

Celaya-Echarri, A., Azpilicueta, L., Aguirre, E., and Falcone, F. (2020). Estimation of electromagnetic field exposure in complex indoor scenarios through hybrid deterministic-stochastic methods. *International Journal of Environmental Research and Public Health*, 17(12), 4482.

Chen, C., Zhang, J., Yuan, J., Liu, Y., and Yan, H. (2023). Electromagnetic fields regulate iron metabolism: From mechanisms to clinical applications. *Heliyon*, 9(3), e14539.

Colombi, D., Thors, B., and Törnevik, C. (2020). Actual power and EMF exposure from base stations in a commercial 5G network. *Applied Sciences*, 10(15), 5280.

Combeau, P., Rostaing, J., Mazet, J., and Sareni, B. (2020). A numerical simulation system for mobile telephony base station EMF exposure using smartphones as probes and a genetic algorithm. *IET Microwaves, Antennas and Propagation*, 14(13), 1587–1594.

De-Sousa, M., Klein,G., Korte,T and Niehaus, M.(2002). Electromagnetic interference in patients with implanted cardioverter-defibrillators and implantable loop recorders. *Indian Pacing Electrophysiology Journal,* 2(3):79–84.

Elbasheir, A. A., Mustapha, A., Hashim, N., and Khatun, S. (2022). Electromagnetic field exposure boundary analysis at the near field for multi-technology cellular base station site. *IET Communications*, 16(17), 2023–2030.

Faruk, S. M., Olowononi, F. D., and Ganiyu, R. A. (2019). A predictive model for assessing path loss in an urban environment: A case study of Ilorin metropolis, Nigeria. *International Journal of Engineering and Technology*, 11(2), 114–120.

Fernández-García, M., Rodríguez-Oramas, C., and García-Carrión, R. (2020). Implications for social impact of dialogic learning. *Frontiers in Psychology*, 11, 628.

Frei, P., Mohler, E., Bürgi, A., Fröhlich, J., Neubauer, G., Braun-Fahrländer, C., and Röösli, M. (2009). A prediction model for personal radio frequency electromagnetic field exposure. *Science of the Total Environment*, 408(1), 102–108.

Ghanem, K., and Vukovic, D. (2020). Assessment of electromagnetic field exposure in urban environments: A case study. *Journal of Electromagnetic Analysis and Applications*, 12(4), 89–98.

Giambene, G., Tavanti, L., and Tarchi, D. (2019). Modeling and planning the next generation cellular networks with EMF constraints. *IEEE Access*, 7, 142184–142198.

Hardell, L.(2017). World Health Organization, radiofrequency radiation and health - a hard nut to crack. *International Journal of Oncology,* 51(2),405–413

Ijabor, B. O., Nwabuoku, A. O., and Izediunor, V. C. (2023). Assessment of radiation risk from selected telecommunication base stations in Ogwashi-Uku, Delta State, Nigeria. *Open Access Library Journal,* 10, 1–13.

Karipidis, K., Mate, M., Sanagou, M., Brzozek, C., Urban, D and Elwood, M.(2021). Mobile phone use and trends in the incidence of cancers of the parotid and other salivary glands. *Cancer Epidemiology*, 73: 101961

Lou, H., Zhou, Y., and Xiao, S. (2021). 5G and EMF exposure: Misinformation, open questions, and potential solutions. *IEEE Access*, 9, 24992–25003.

Miller, A.B., Sears , M.E., Morgan, L.L., Davis , Hardell,L., Oremus, M. and Soskolne, C.L.(2019). Risks to health and well-being from radio-frequency radiation emitted by cell phones and other wireless devices. *Front Public Health,* 13(7),223

Nyakyi, C. P., Mpeshe, S. C., and Dida, M. (2024). Optimization of RF-EMF exposure to public in Tanzania using artificial neural network and multi-linear regression models. *Environmental Challenges*, 9, 100532.

Okelola, M.O and Olabode, O.E. (2018). Detection of voltage unbalance on three-phase induction motor using artificial neural network. *International Journal of Emerging Trends in Engineering and Development*,4(8),18-25

Olabode, O.E., Akinyele, D.O., Ariyo, F.K., Raji, A.A., Omoniyi, E.B., and Akinde, O.K. (2024). Optimal performance of multiple energy sources under varying dispatch strategies on a 4g base transceiver station. *Journal of Sustainable Energy,* 15(2), 77-93

Pravir, K., Khatun, F., and Aziz, M. A. (2021). Overview of the evaluation methods for the maximum EMF exposure in 5G networks. *Optik*, 228, 166155.

Ramirez-Vazquez, R., Escobar, I., Vandenbosch, G. A. E., and Arribas, E. (2024). Personal exposure to radiofrequency electromagnetic fields: A comparative analysis of international, national, and regional guidelines. *Environmental Research*, 246, 118124.

Sheng, J., Amankwah-Amoah, J and Wang, X. (2019). Technology in the 21st century: new challenges and opportunities. *Technological Forecasting and Social Change*, 143:321-335

Suarez, A., Emfietzoglou, D., and Domenech, M. (2023). Survey of RF electromagnetic field exposure in a public health research environment. *Bioelectromagnetics*, 44(5), 432–440.

Tera, S.P., Chinthaginjala, R., Pau, G. and Hoon Kim, T. (2025). Toward 6G: an overview of the next generation of intelligent network connectivity. in *IEEE Access*, 13: 925-961.